Version: 1.21

Search for the Higgs boson
in $H \rightarrow WW^{(*)} \rightarrow \ell\ell'$ $(\ell, \ell' = e, \mu)$ decays with 1.2 fb^{-1} at DØ in Run IIb

The DØ Collaboration
URL http://www-d0.fnal.gov
(Dated: March 6, 2008)

A search for the Standard Model Higgs boson is presented in $H \rightarrow WW^{(*)} \rightarrow \ell\ell'$ $(\ell, \ell' = e, \mu, \tau)$ decays in $p\bar{p}$ collisions at a center-of-mass energy of $\sqrt{s} = 1.96$ TeV. Final states containing either two electrons e^+e^-, an electron and a muon $e^{\pm}\mu^{\mp}$ or two muons $\mu^+\mu^-$ have been considered. The data sample used in this analysis has been collected between June 2006 and July 2007 by the DØ detector during Run IIb of the Fermilab Tevatron collider and corresponds to an integrated luminosity of 1.2 fb^{-1}. No significant excess above the background has been observed, and upper limits on the production cross section times branching ratio $\sigma \times BR(H \rightarrow WW^{(*)})$ are presented on the combination of the three channels. Finally, these analyses are combined with the previous ones performed with Run IIa data.

Preliminary Results for Moriond - Winter 2008

I. INTRODUCTION

In the Standard Model (SM), the Higgs boson is crucial to the understanding of electroweak symmetry breaking and the mass generation of electroweak gauge bosons and fermions. Direct searches at the CERN e^+e^- collider (LEP) yield a lower limit for the Higgs boson mass of $m_H > 114.4$ GeV [1] at 95% confidence level (CL). Indirect measurements via fits to the electroweak precision data give an upper bound of $m_H < 182$ GeV [2] at 95% CL when taken together with the direct lower limit.

In this note a search for Higgs bosons decaying to the $WW^{(*)}$ final state in the DØ experiment at the Tevatron is presented. To achieve a good signal-to-background ratio, the leptonic decay modes $H \to WW^{(*)} \to \ell\ell'$ ($\ell, \ell' = e, \mu, \tau$) are considered, leading to final states containing either two electrons e^+e^-, an electron and a muon $e^\pm\mu^\mp$, or two muons $\mu^+\mu^-$, and missing transverse momentum ($\not{E}_T$). (The τ must decay leptonically to either a muon or electron in order to contribute.) This decay mode provides the largest sensitivity for the SM Higgs boson search at the Tevatron at a Higgs boson mass of $m_H \sim 160$ GeV [3–5]. If combined with searches exploiting the WH and ZH associated production, this decay mode also increases the sensitivity for the Higgs boson searches in the low mass region, $m_H \sim 120$ GeV.

Upper limits on the $H \to WW^{(*)} \to \ell\ell'$ cross section times branching ratio from the previous Run IIa data set have already been presented in Ref. [6, 7]. In the present analysis, the most recent DØ data available is analyzed, from Run IIb. Upper limits on $\sigma(H) \times BR(H \to WW^{(*)})$ are presented using the combination of these three di-lepton channels. Finally, the analyses are combined with the previous Run IIa analyses.

II. DØ DETECTOR

We briefly describe the main components of the DØ Run II detector [8] important to this analysis. The central tracking system consists of a silicon microstrip tracker (SMT) and a central fiber tracker (CFT), both located within a 2.0 T axial magnetic field. The SMT strips have a typical pitch of 50–80 μm, and the design is optimized for tracking and vertexing over the pseudorapidity range $|\eta| < 3$, where $\eta = -\ln(\tan\frac{\theta}{2})$ with polar angle θ. The system has a six-barrel longitudinal structure, with each barrel a set of four silicon layers arranged axially around the beam pipe, interspersed with sixteen radial disks. In addition, a new layer of silicon (Layer 0) has been added just outside the beampipe for Run IIb. The CFT has eight thin coaxial barrels, each supporting two doublets of overlapping scintillating fibers of 0.835 mm diameter, one doublet parallel to the beam axis, the other alternating by $\pm3°$ relative to the beam axis.

A liquid-argon/uranium calorimeter surrounds the central tracking system and consists of a central calorimeter (CC) covering to $|\eta| \approx 1.1$, and two end calorimeters (EC) extending coverage for $|\eta| < 4.2$, each housed in separate cryostats [9]. Scintillators between the CC and EC cryostats provide sampling of showers for $1.1 < |\eta| < 1.4$.

The muon system is located outside the calorimeters and consists of a layer of tracking detectors and scintillation trigger counters inside toroid magnets which provide a 1.8 T magnetic field, followed by two similar layers behind each toroid. Tracking in the muon system for $|\eta| < 1$ relies on 10 cm wide drift tubes [9], while 1 cm mini-drift tubes are used for $1 < |\eta| < 2$ [10].

III. DATA AND MC SAMPLES

The data sample used in this analysis has been collected between June 2006 and July 2007 (Run IIb) by the DØ detector at the Fermilab Tevatron collider at $\sqrt{s} = 1.96$ TeV, corresponding to an integrated luminosity of 1.2 ± 0.07 fb^{-1}. For the ee ($\mu\mu$) final state, the normalization is a factor that scales the NNLO $Z/\gamma^* \to ee$ ($\mu\mu$) cross section to the data in the mass region $60 < M_{\ell\ell} < 130$ GeV. For the $e\mu$ final state, the simulations are normalized by the factor needed to scale the mass distribution from the NNLO $Z/\gamma^* \to \tau\tau$ cross section to data. Data/MC electron and muon correction factors were applied to MC before normalization factors were measured. The estimated data samples were found to be consistent with the measurement of 1.2 fb^{-1} from the luminosity system within $\pm5\%$. Some systematic uncertainties, coming from the luminosity determination or data/MC correction factors are canceled by using such a normalization procedure.

The signal and SM background processes have been simulated with PYTHIA 6.323 [11] (except for W/Z+jets in the $\mu\mu$ channel, where ALPGEN [12] is used instead) using the CTEQ6.1M [13] parton distribution functions, followed by a detailed GEANT-based [14] simulation of the DØ detector. The $Z/\gamma^* \to \ell\ell$ cross section is calculated with CTEQ6.1M PDFs as $\sigma(Z/\gamma^* \to \ell\ell) = \sigma_{LO} \times K_{QCD}(Q^2)$, with the LO cross section calculated by Pythia LO PDF and the K_{QCD} at NNLO with NLO PDF, calculated according to [15, 16]. The cross section times branching ratio of

$Z/\gamma^* \to \ell\ell$ production in the invariant mass region 60 GeV $< M_{ll} <$ 130 GeV is $\sigma \times BR = 241.6$ pb. The $Z + jets$ events are also re-weighted to the Z $p_{\rm T}$ distribution observed in data.

The $W \to l\nu$ background level is calculated with NNLO corrections and CTEQ6.1M as listed in [16]. For inclusive W boson production with decays into a single-flavor lepton state this value is $\sigma \times BR = 2583$ pb. The calculations of Ref. [17] are used for $t\bar{t}$ production with $\sigma \times BR = 0.076$ pb with single-flavor lepton decays of both W bosons. The NLO WW, WZ and ZZ production cross section values are taken from Ref. [18] with $\sigma \times B = 0.15$ pb for WW, $\sigma \times B = 0.014$ pb for WZ and $\sigma \times B = 0.002$ pb for ZZ production with decay into a single-flavor lepton state.

The background due to multijet production (called QCD fakes), when jets are misidentified as leptons, is determined from the data. A sample of like-sign di-lepton events is used in the $\mu\mu$ channel, corrected for like-sign contributions from other processes. The other channels use events with inverted lepton quality cuts, corrected to match the normalization and kinematics determined in the like-sign data.

IV. EVENT SELECTION

The $H \to WW^{(*)} \to \ell\ell'$ ($\ell, \ell' = e, \mu, \tau$) candidates are selected by triggering on single or di-lepton events using a three level trigger system. The first trigger level uses hardware to select electron candidates based on energy deposition in the electromagnetic part of the calorimeter and muon candidates formed by hits in the muon system. Later versions of the trigger also require a high $p_{\rm T}$ central track reconstructed in the CFT by the specialized central track trigger (CTT). Digital signal processors in the second trigger level form muon track candidate segments defined by hits in the muon drift chambers and scintillators, as well as match lepton candidates to a more precise central track using additional SMT hits reconstructed by the silicon track trigger (STT). At the third level, software algorithms running on a computing farm and exploiting the full event information are used to make the final selection of events which are recorded.

In the further offline analysis, electrons are identified by using calorimeter and tracking information. Electromagnetic showers are identified in the calorimeter by comparing the longitudinal and transverse shower profiles to those of simulated electrons. The showers must be isolated, deposit most of their energy in the electromagnetic part of the calorimeter and pass a likelihood criterion that includes a spatial track match and, in the central detector region, an E/p requirement, where E is the energy of the calorimeter cluster and p is the momentum of the track. Electrons must be reconstructed within a detector pseudorapidity $|\eta| < 3.0$. The transverse momentum measurement of the electrons is based on calorimeter cell energy information. An electron likelihood is used to further enhance the purity of the electron sample and to reduce the rate of jets misidentified as electrons.

Muon tracks are reconstructed from hits in the wire chambers and scintillators in the muon system and must match a track in the central tracker. To select isolated muons, the scalar sum of the transverse momentum of all tracks, other than that of the muon, in a cone of $\mathcal{R} = 0.5$ around the muon track is calculated, where $\mathcal{R} = \sqrt{(\Delta\phi)^2 + (\Delta\eta)^2}$ and ϕ is the azimuthal angle. The transverse energy deposited in the calorimeter in a hollow cone of $0.1 < \mathcal{R} < 0.4$ around the muon is also measured. In the $e\mu$ final state, both quantities are required to be < 2.5 or 4.0 GeV, depending on the Higgs mass. In the $\mu\mu$ final state, the sum of the variables divided by the muon $p_{\rm T}$ (scalediso) is required to be < 0.4 (0.5) for the leading (trailing) muon, and their product < 0.06. Muons are restricted to the fiducial coverage of the muon system $|\eta| < 2.0$. Muons from cosmic rays are rejected by requiring a timing criterion on the hits in the scintillator layers as well as applying restrictions on the position of the muon track with respect to the selected primary vertex.

In all final states, two leptons originating from the same primary vertex are required to be of opposite charge. They must have $p_T^e > 20$ GeV for the leading electron and $p_T^e > 15$ GeV for the trailing one in the ee channel, $p_T^e > 15$ GeV for the electron and $p_T^\mu > 10$ GeV for the muon in the $e\mu$ final state and $p_T^\mu > 10$ GeV for the leading and trailing muons in the $\mu\mu$ final state. In addition, the di-lepton invariant mass is required to exceed 15 GeV. This stage of the analysis is referred to as "pre-selection".

At this stage, the background is dominated by Z/γ^* production which is suppressed by requiring missing transverse energy. Events are further removed if the $\not{E}_T$ could have been produced by a mis-measurement of jet energies. The fluctuation in the measurement of jet energy in the transverse plane can be approximated by $\Delta E^{\rm jet} \cdot \sin\theta^{\rm jet}$ where $\Delta E^{\rm jet}$ is proportional to $\sqrt{E^{\rm jet}}$. The opening angle $\Delta\phi\,({\rm jet}, \not{E}_T)$ between this projected energy fluctuation and the missing transverse energy provides a measure of the contribution of the jet to the missing transverse energy. The scaled missing transverse energy is defined as:

$$\not{E}_T^{\rm Scaled} = \frac{\not{E}_T}{\sqrt{\sum_{\rm jets}\left(\Delta E^{\rm jet} \cdot \sin\theta^{\rm jet} \cdot \cos\Delta\phi\,({\rm jet}, \not{E}_T)\right)^2}} \tag{1}$$

The minimal transverse mass is defined as:

$$M_T^{min}(l, \not{E}_T) = \sqrt{2p_T^l \not{E}_T (1 - \cos \Delta\phi(l, \not{E}_T))} \tag{2}$$

and is required to be large in order to suppress background where the $\not{E}_T$ is coming from mis-measured lepton energy. Z/γ^* boson and multi-jet events can be rejected with a cut on the opening angle $\Delta\phi_{\ell\ell}$, since most of the background decays are back-to-back. This is not the case for Higgs boson decays because of the spin correlations from the scalar decay. Finally, $t\bar{t}$ events are further rejected by a cut on H_T, the scalar sum of the p_T of good jets in the event.

Many selections are Higgs mass and final-state dependent and optimized to further suppress contributions from Z/γ^*, di-boson (WW, WZ, ZZ), $W(\to \ell\nu) + jets$, and multijet backgrounds. Figure 1 shows the invariant ee mass, $\not{E}_T$, $\not{E}_T^{\text{Scaled}}$, M_T^{min}, $\sum p_T = p_T^{e_1} + p_T^{e_2} + \not{E}_T$, and H_T distributions in data, backgrounds, and signal at pre-selection, for the ee channel. Table I shows the cuts used for a selection of Higgs masses in the ee channel; cuts were optimized for each Higgs mass in 10 GeV steps. Figure 2 shows the comparison between data and MC for the invariant mass of the $e\mu$ system and for the missing transverse energy at the pre-selection level, for the $e\mu$ channel. Further cuts have been optimized for each Higgs mass in the $e\mu$ channel, and a sample of them are given in Table II. Figure 3 shows the comparison between data and Monte Carlo for the invariant mass of the $\mu\mu$ system and the missing transverse energy at the pre-selection level, for the $\mu\mu$ channel. The same cuts were found to be optimal for all Higgs masses in the $\mu\mu$ channel, as shown in Table III. Table IV shows the number of expected and observed events after pre-selection and final selections (the NN input stage), for all three channels.

Selection criteria	$m_H = 115$ GeV	$m_H = 160$ GeV	$m_H = 200$ GeV
Cut 0 Pre-selection	lepton ID, leptons with opposite charge and $p_T^{e_1} > 20$ GeV and $p_T^{e_2} > 15$ GeV invariant mass $M_{ee} > 15$ GeV		
Cut 1 Missing Transverse Energy $\not{E}_T$ (GeV)	> 20	> 20	> 20
Cut 2 $\not{E}_T^{\text{Scaled}}$	> 6	> 7	> 7
Cut 3 M_T^{min} $(\ell, \not{E}_T)$ (GeV)	> 35	> 50	> 50
Cut 4 Sum of $p_T^\ell + p_T^{\ell'} + \not{E}_T$ (GeV)	80-120	90-160	120-200
Cut 5 Invariant mass M_{ee} (GeV)	< 40	< 70	< 75
Cut 6 H_T (GeV)	< 50	< 80	< 80
Cut 7 $\Delta\phi(e_1, e_2)$	< 2.5	< 2.0	< 2.0

TABLE I: Summary of the selection criteria for various Higgs masses in the ee channel.

Selection criteria	$m_H = 115$ GeV	$m_H = 160$ GeV	$m_H = 200$ GeV
Cut 0 Preselection	lepton ID, leptons with opposite charge and $p_T^e > 15$ GeV and $p_T^\mu > 10$ GeV invariant mass $M_{e\mu} > 15$ GeV		
Cut 1 Missing Transverse Energy $\not{E}_T$ (GeV)	> 20	> 20	> 20
Cut 2 $\not{E}_T^{\text{Scaled}}$	> 7	> 7	> 7
Cut 3 M_T^{min} $(\ell, \not{E}_T)$ (GeV)	> 45	> 65	> 65
Cut 4 Invariant mass $M_{e\mu}$ (GeV)	< 60	< 80	< 100
Cut 5 H_T (GeV)	< 70	< 70	< 70
Cut 6 $\Delta\phi(e, \mu)$	< 1.25	< 2.5	< 2.5

TABLE II: Summary of the selection criteria for various Higgs masses in the $e\mu$ channel.

Selection criteria	$m_H = 115$ GeV	$m_H = 160$ GeV	$m_H = 200$ GeV
Cut 0 Preselection	lepton ID, leptons with opposite charge and $p_T^{\mu 1} > 10$ GeV and $p_T^{\mu 2} > 10$ GeV invariant mass $M_{\mu\mu} > 15$ GeV		
Cut 1 Missing Transverse Energy $\not{E}_T$ (GeV)	> 20	> 20	> 20
Cut 2 $\not{E}_T^{\text{Scaled}}$	> 5	> 5	> 5
Cut 3 M_T^{min} $(\ell, \not{E}_T)$ (GeV)	> 20	> 20	> 20
Cut 4 $\Delta\phi(\mu, \mu)$	< 2.5	< 2.5	< 2.5

TABLE III: Summary of the selection criteria for various Higgs masses in the $\mu\mu$ channel.

	ee pre-selection	ee final	$e\mu$ pre-selection	$e\mu$ final	$\mu\mu$ pre-selection	$\mu\mu$ final
$Z \to ee$	48785 ± 123	0.8 ± 0.6	138 ± 8.2	0 ± 0	-	-
$Z \to \mu\mu$	-	-	76.4 ± 4.2	0.39 ± 0.25	109122 ± 230	632.6 ± 10.6
$Z \to \tau\tau$	230.4 ± 7.1	0 ± 0	884 ± 14.5	0 ± 0	998 ± 27.2	30.8 ± 2.4
$t\bar{t}$	26.7 ± 0.7	0.75 ± 0.1	62.6 ± 1.1	2.4 ± 0.2	44.8 ± 0.6	25.1 ± 0.4
$W + jets$	16.6 ± 2.7	1.5 ± 1.0	60.5 ± 5.3	3.0 ± 1.1	97.9 ± 9.8	66.7 ± 9.7
WW	37.5 ± 1.0	7.4 ± 0.4	97.8 ± 1.7	14.6 ± 0.6	78.0 ± 0.4	46.2 ± 0.4
WZ	35.6 ± 1.4	0.07 ± 0.05	6.9 ± 0.6	0.66 ± 0.18	36.5 ± 1.0	8.72 ± 0.6
ZZ	26.7 ± 0.7	0.14 ± 0.05	1.78 ± 0.2	0.02 ± 0.02	41.2 ± 0.8	7.19 ± 0.3
Multijet	147 ± 280	0.04 ± 0.7	108 ± 130	0 ± 0.5	263 ± 92.5	14.5 ± 2.1
Signal ($m_H = 160$ GeV)	1.34 ± 0.03	0.82 ± 0.02	3.58 ± 0.05	1.76 ± 0.04	3.52 ± 0.08	2.08 ± 0.03
Total Background	49306 ± 306	$10.7 \pm 1.7 \pm 1.7$	1436 ± 138	$21.1 \pm 1.3 \pm 3.4$	110681 ± 231	$831.8 \pm 29 \pm 34$
Data	50593	10.0	1424	18	109918	839

TABLE IV: Expected and observed number of events in each channel after pre-selection and final selections (the NN input stage). Statistical uncertainties in the expected yields are shown for all backgrounds, and the systematic uncertainty is also shown as the second value for the total background.

V. MULTIVARIATE DISCRIMINANTS

To improve the separation of signal from backgrounds, an artificial neural network (NN) is used in each of the three di-lepton channels. The NN's were trained using approximately half of the background and signal events, the rest being used to test the networks' performance and to compare with data. A separate NN is trained for each Higgs boson mass tested. In the $\mu\mu$ channel, a weighted sum of all backgrounds was used during training. For the ee and $e\mu$ channels the NN was trained only against the main $W + jets$ and WW backgrounds.

A list of input variables has been derived based on the separation power of the various distributions, for each of the three channels. Those variables can be divided into three classes, object kinematics, event kinematics and angular variables. One of the input variables is a discriminant constructed using the Matrix Element (ME) method. Leading-order parton states for either signal ($H \to WW$) or WW background are integrated over, with each state weighted according to its probability to produce the observed measurement. A Data to MC comparison of the ME discriminant in the ee channel at pre-selection level and after final selections can be found in Figure 5. The NN input variables for the ee and $e\mu$ channel are listed in Table V and those for the $\mu\mu$ channel in Table VI. The NN output for $m_H = 160$ GeV is displayed in Figures 6, 7, and 8 for the ee, $e\mu$, and $\mu\mu$ channels, respectively.
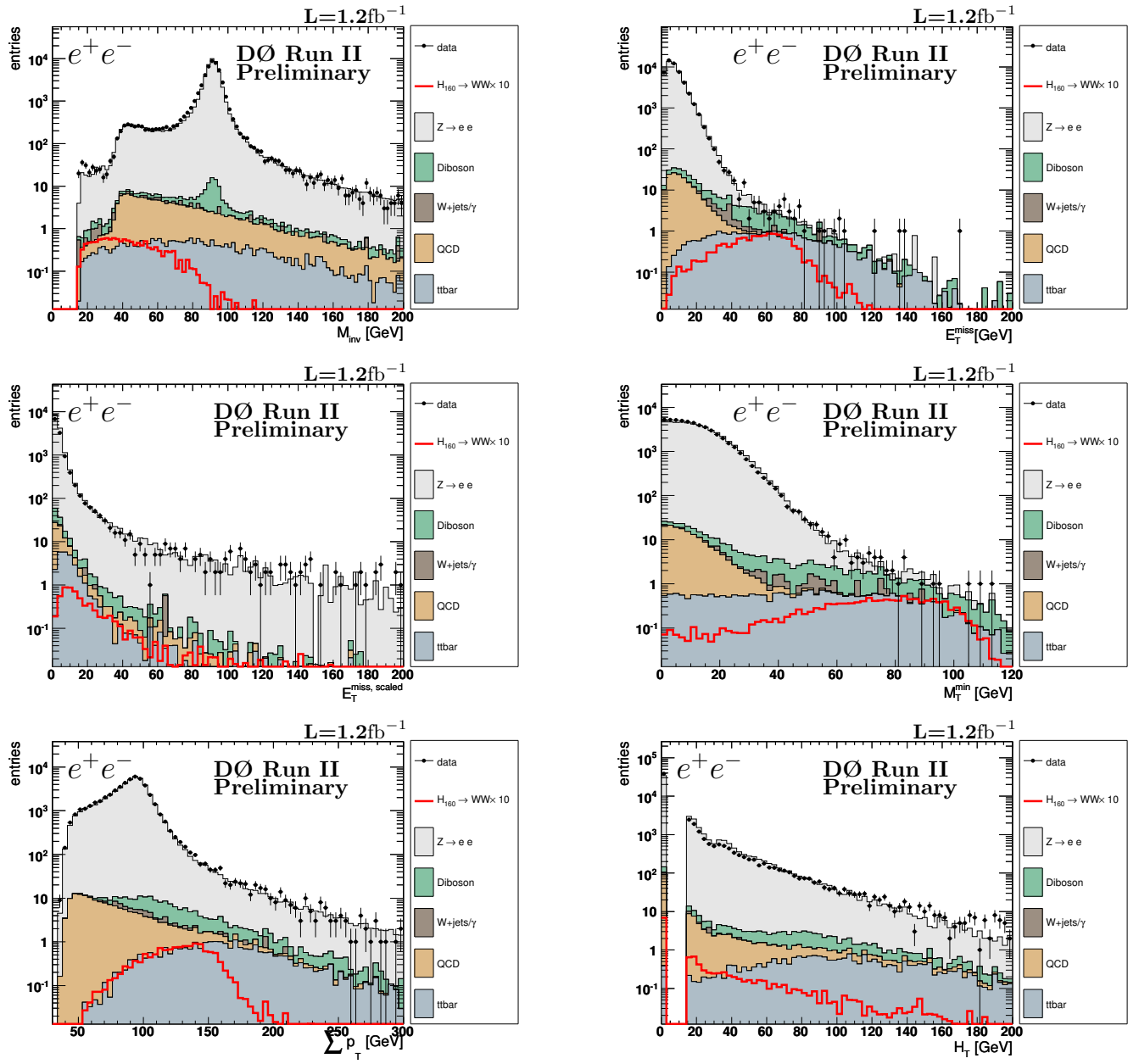
FIG. 1: Distributions at pre-selection of: *ee* mass (top left), $\not{E}_T$ (top right), $\not{E}_T^{\text{Scaled}}$ (middle left), M_T^{min} (middle right), $\sum p_T$ (bottom left), H_T (bottom right), for data (points with error bars), background simulation (histograms, complemented with the QCD expectation) and signal expectation times 10 for $m_H = 160$ GeV (solid line).
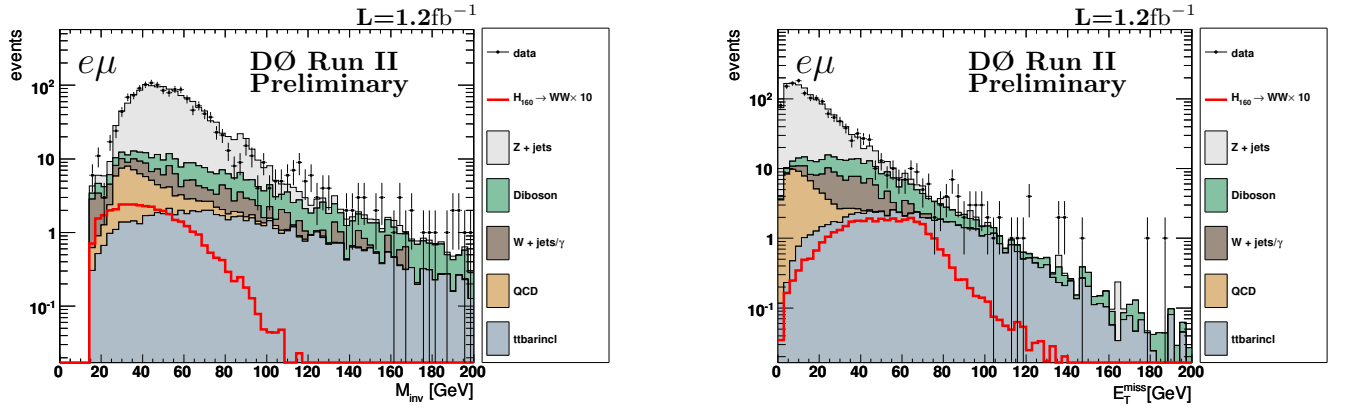
FIG. 2: Distribution of the invariant mass $M_{e^{\pm}\mu^{\mp}}$ (left) and $\not{E}_T$ (right) at pre-selection for the $e\mu$ channel.
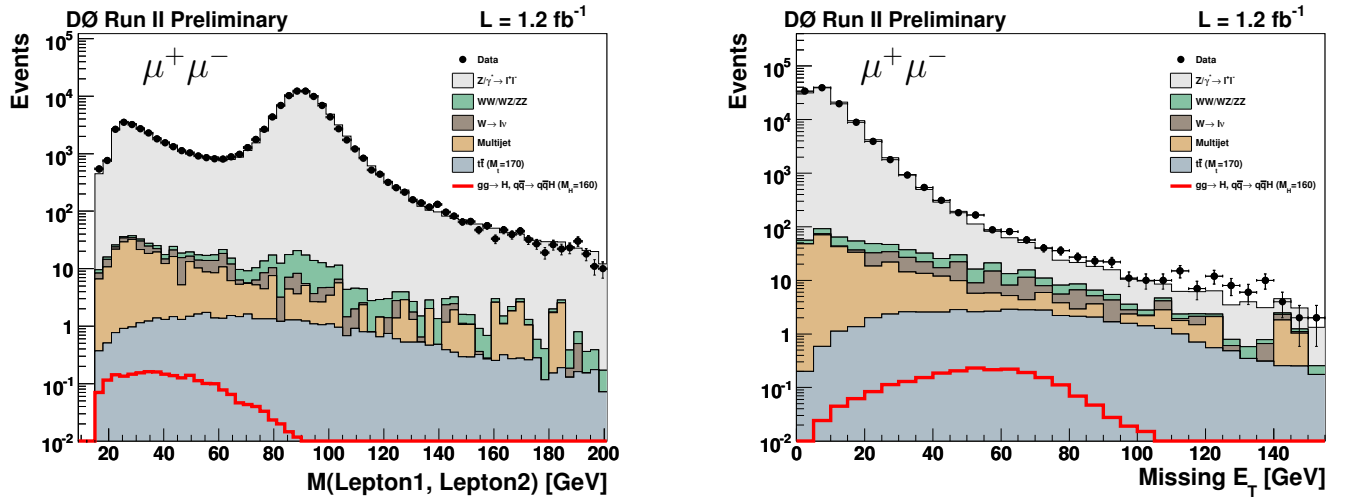

FIG. 3: Distribution of the invariant mass $M_{\mu^+\mu^-}$ (left) and $\not{E}_T$ (right) at pre-selection for the $\mu\mu$ channel.
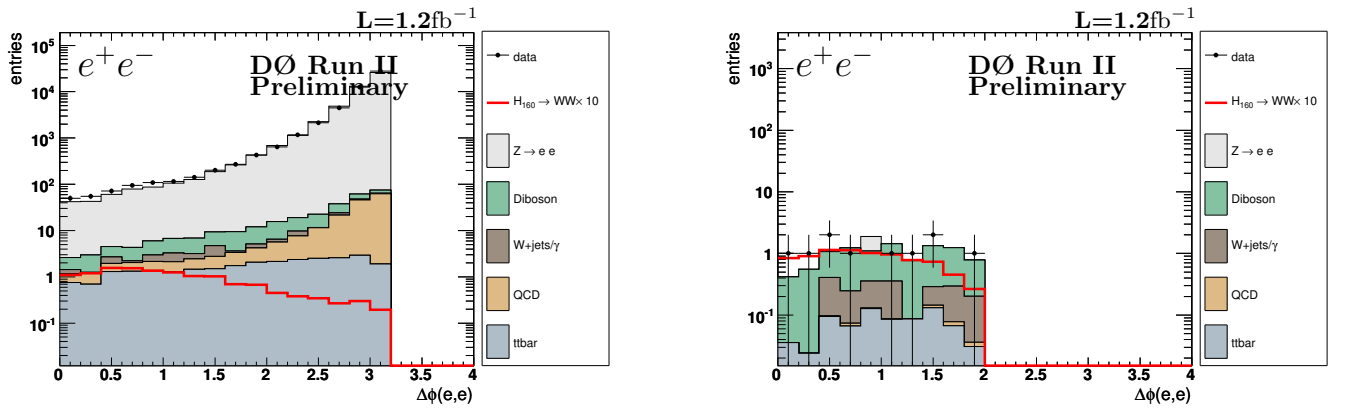

FIG. 4: Distribution of $\Delta\phi(e_1, e_2)$ after pre-selection (left) and final selection (right), in the ee channel.
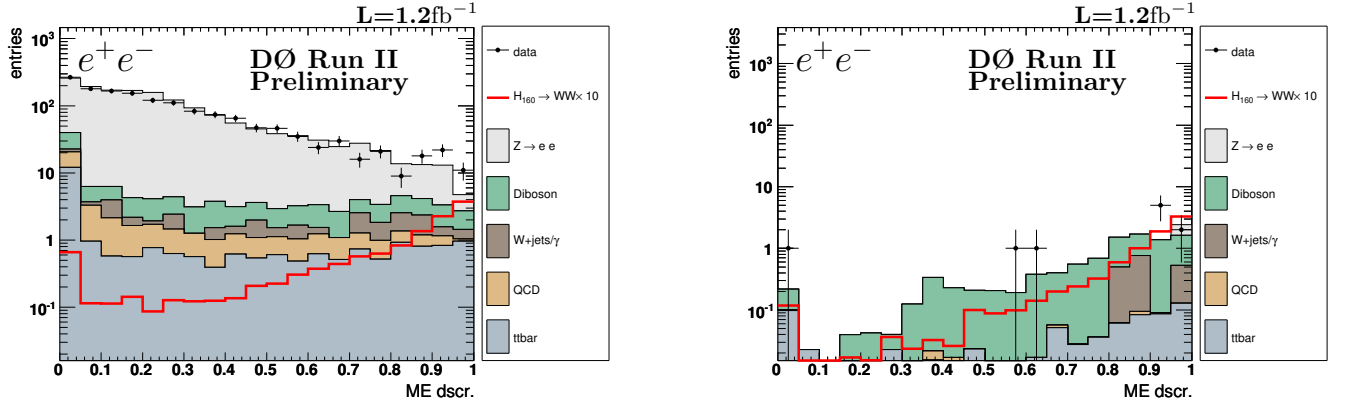
FIG. 5: Distribution of the ME discriminant after pre-selection (left) and final selection (right), in the ee channel.

ee / $e\mu$ NN Analysis Variables	
p_T of leading lepton	$p_T(\ell_1)$
p_T of trailing lepton	$p_T(\ell_2)$
Sum of the transverse momenta of the leptons:	$p_T(\ell_1) + p_T(\ell_2)$
Invariant mass of both leptons	$M_{\mathrm{inv}}(\ell_1, \ell_2)$
Minimal transverse mass of one lepton and $\not{E}_T$	M_T^{min}
Missing transverse energy	$\not{E}_T$
Azimuthal angle between selected leptons	$\Delta\phi(\ell_1, \ell_2)$
Solid angle between selected leptons	$\Theta\phi(\ell_1, \ell_2)$
ΔR between selected leptons	$\Delta R(\ell_1, \ell_2)$
Azimuthal angle between leading lepton and $\not{E}_T$	$\Delta\phi(\not{E}_T, \ell_1)$
Azimuthal angle between trailing lepton and $\not{E}_T$	$\Delta\phi(\not{E}_T, \ell_2)$
Matrix Element Discriminant	ME_{disc} (not used for $e\mu$)

TABLE V: Input variables for the NN in the ee and $e\mu$ channels.

$\mu\mu$ NN Analysis Variables	
Scaled $\not{E}_T$	$\not{E}_T^{\mathrm{Scaled}}$
Invariant mass of the two muons	$M_{\mu\mu}$
Missing E_T	$\not{E}_T$
Sum of the p_T's of all 0.5 cone jets with $p_T > 6$ GeV	H_T^{all}
$H \to WW$ vs. WW ME discriminant	ME_{disc}
p_T of the $\mu\mu$ system	$p_T(\mu_1 + \mu_2)$
Smaller of the two muon-$\not{E}_T$ transverse masses	M_T^{min}
p_T of the leading p_T muon	$p_T(\mu_1)$
Azimuthal angle between the $\not{E}_T$ and the second-leading p_T muon	$\Delta\phi(\mu_2, \not{E}_T)$
$\log_{10}$ of the sum of the muon scaled (track+cal) isolations	$\log_{10}(\mathrm{scalediso}\ \mu_1 + \mu_2)$
Event scalar E_T	SE_T
Azimuthal angle between the two muons	$\Delta\phi(\mu_1, \mu_2)$
Worst of the two muon qualities (loose,medium,tight)	$\min(\mu_1^{\mathrm{qual}}, \mu_2^{\mathrm{qual}})$
Azimuthal angle between the $\not{E}_T$ and the leading p_T muon	$\Delta\phi(\mu_1, \not{E}_T)$
p_T of the second-leading p_T muon	$p_T(\mu_2)$

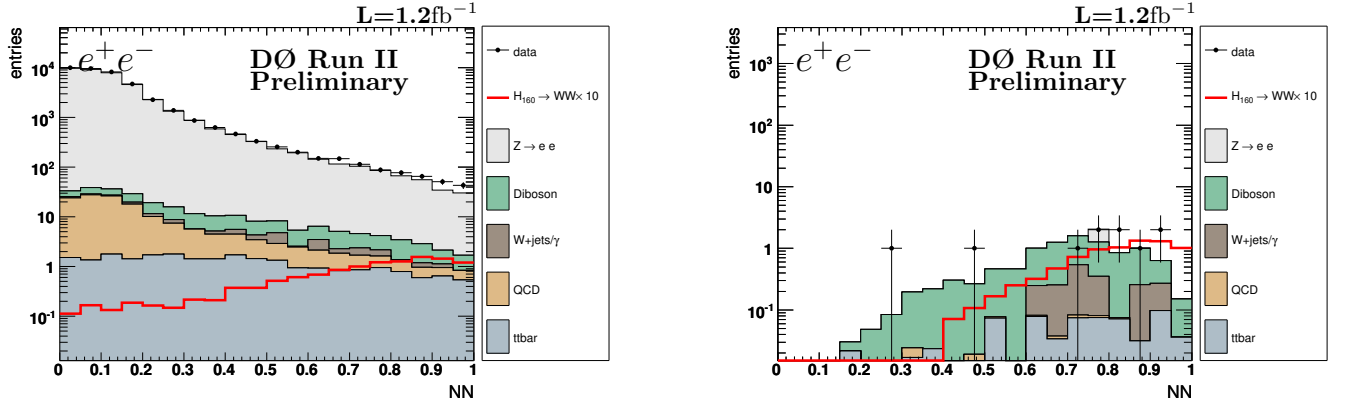TABLE VI: Input variables for the NN in the $\mu\mu$ channels.

FIG. 6: Distribution of the NN output at pre-selection (left) and after the final selection (right) in the ee channel.
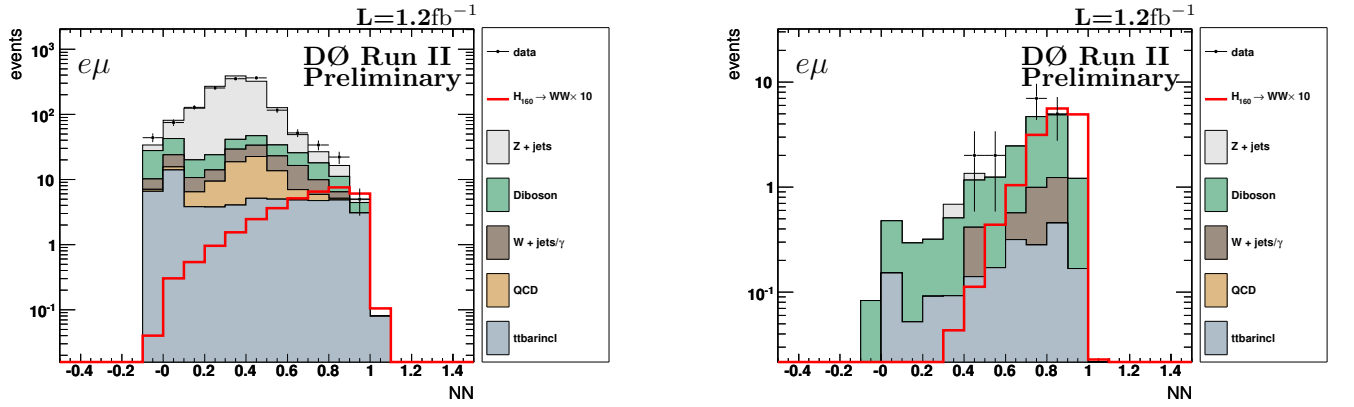

FIG. 7: Distribution of the NN output at pre-selection (left) and after the final selection (right) in the $e\mu$ channel.

VI.   RESULTS AND SUMMARY

The estimates for the expected number of background and signal events depend on numerous factors that each introduce a systematic uncertainty: lepton reconstruction efficiencies (8-13%), trigger efficiencies (5%), jet energy scale calibration (1%), lepton momentum calibration (11%), PDF uncertainties ($< 4\%$), theoretical cross section (di-boson 7%, $t\bar{t}$ 16%), and modeling of multijet background (30%). The systematic uncertainty on the luminosity is mainly a combination of the PDF uncertainty, uncertainty for the NNLO Z cross section (4%) and data/MC normalization factors (2%). The total uncertainty on the background level is approximately 16% and for the signal efficiency is 10%. The effects of these uncertainties on the NN output distribution shapes were also studied and included as additional systematic uncertainties. Further NN output shape uncertainties were included based on the agreement of NN input variables between data and MC at pre-selection and the difference in WW p_{T} between Pythia and Sherpa [19].

After all selection cuts, the NN output distributions of data agree within uncertainties with the expected backgrounds. Thus the NN output distributions are used to set limits on the production cross section times branching ratio $\sigma \times BR(H \to WW^{(*)})$. We calculate limits for each channel and all three channels combined, using the CLs method with a log-likelihood ratio (LLR) test statistic [20]. To minimize the degrading effects of systematics on the search sensitivity, the individual background contributions are fitted to the data observation by maximizing a profile likelihood function for each hypothesis [21]. Table VII presents expected and observed upper limits at 95% CL for $\sigma \times BR(H \to WW^{(*)})$ relative to that expected in the SM, for each of the three final states, all three combined, the Run IIa data alone, and these Run IIb analyses combined with Run IIa, for each Higgs boson mass considered.
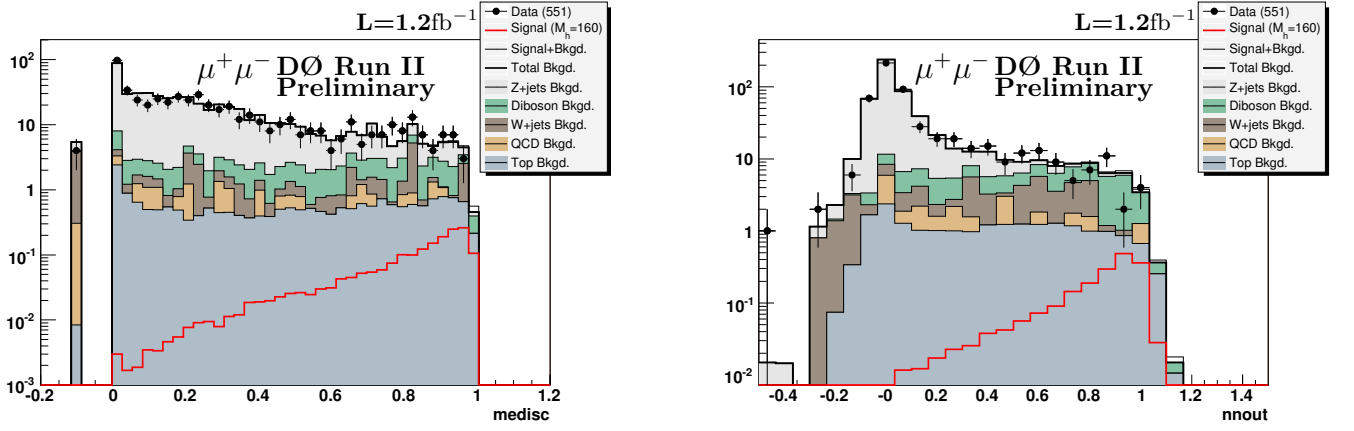
FIG. 8: Distribution of the ME discriminant (left) and the NN output (right) after the final selection in the $\mu\mu$ channel. Values of $ME_{disc} < 0$ correspond to events which were found to have very small probability for either signal or WW background.

TABLE VII: Expected and observed upper limits at 95% CL for $\sigma \times BR(H \to WW^{(*)})$ relative to the SM for e^+e^-, $e\mu$, and $\mu^+\mu^-$ final states in Run IIb, their combination, the Run IIa combined analyses, and finally Run IIa and Run IIb analyses combined, for different Higgs boson masses (m_H).

$m_H=$	115	120	125	130	135	140	145	150	155	160	165	170	175	180	185	190	195	200
$e\mu$ (exp.)	91.17	43.62	31.55	21.55	17.40	14.81	13.33	9.22	7.33	5.11	5.19	5.99	7.07	7.72	10.93	13.03	14.76	16.47
$e\mu$ (obs.)	103.99	41.02	29.39	23.58	15.64	15.31	13.20	8.10	7.17	3.84	5.32	5.16	7.35	8.37	10.19	12.21	15.73	14.60
ee (exp.)	194.50	70.72	54.72	28.50	31.17	20.14	16.51	15.43	12.65	8.20	8.67	10.03	11.08	12.72	16.09	20.78	26.40	32.36
ee (obs.)	172.61	109.91	70.77	41.14	42.30	30.42	17.54	18.78	12.90	12.85	12.39	14.24	18.57	17.97	21.16	25.71	23.45	33.17
$\mu\mu$ (exp.)	56.06	33.80	24.21	20.56	14.75	13.71	11.79	10.74	8.89	7.63	6.80	8.70	9.30	10.53	13.15	17.24	19.54	27.05
$\mu\mu$ (obs.)	92.73	66.22	45.41	20.75	18.54	15.65	12.10	11.80	7.53	7.48	6.53	7.39	7.83	8.77	9.54	12.00	14.45	26.45
All (exp.)	48.08	23.53	18.33	12.65	11.00	8.76	7.70	6.36	4.99	3.54	3.46	4.32	4.75	5.40	7.10	9.18	10.51	13.52
All (obs.)	72.37	44.3	30.26	15.96	13.49	12.28	8.01	6.85	4.51	3.53	4.20	3.88	5.75	5.80	6.38	7.64	8.37	11.97
Run IIa (exp.)	-	25.73	17.31	12.37	9.77	8.47	6.47	5.23	4.27	3.40	3.77	4.15	4.66	5.15	6.27	7.51	9.34	10.65
Run IIa (obs.)	-	49.62	29.60	21.78	16.10	11.66	6.92	5.17	4.63	2.97	3.46	4.18	4.23	5.40	5.31	5.46	11.88	8.19
Run II (exp.)	48.08	16.85	12.75	8.82	7.46	6.01	4.98	4.08	3.17	2.39	2.42	2.90	3.22	3.63	4.64	5.78	6.90	8.68
Run II (obs.)	72.37	40.77	26.10	15.66	12.29	9.88	5.47	4.31	3.21	2.12	2.65	2.59	3.51	3.93	3.84	4.21	7.07	6.54

Figure 9 shows the expected and observed limits for $\sigma \times BR(H \to WW^{(*)})$ relative to the SM for the different Higgs boson masses and the LLR distribution for the 1.2 fb^{-1} of Run IIb data. Figure 10 shows the same, but after combining with the Run IIa analyses, thus for the full Run II dataset of 2.3 fb^{-1}. So far, no region of the SM Higgs mass range can be excluded, and no significant excess is observed.

[1] R. Barate *et al.*, Phys. Lett. B **565**, 61 (2003).
[2] The LEP Electroweak Working Group, *Precision Electroweak Measurements and Constraints on the Standard Model*, arXiv:0712.0929 [hep-ex].
[3] T. Han, A. Turcot, R-J. Zhang, Phys. Rev. D **59**, 093001 (1999).
[4] M. Carena *et al.* [Higgs Working Group Collaboration], "Report of the Tevatron Higgs working group", hep-ph/0010338.
[5] K. Jakobs, W. Walkowiak, ATLAS Physics Note, ATL-PHYS-2000-019.
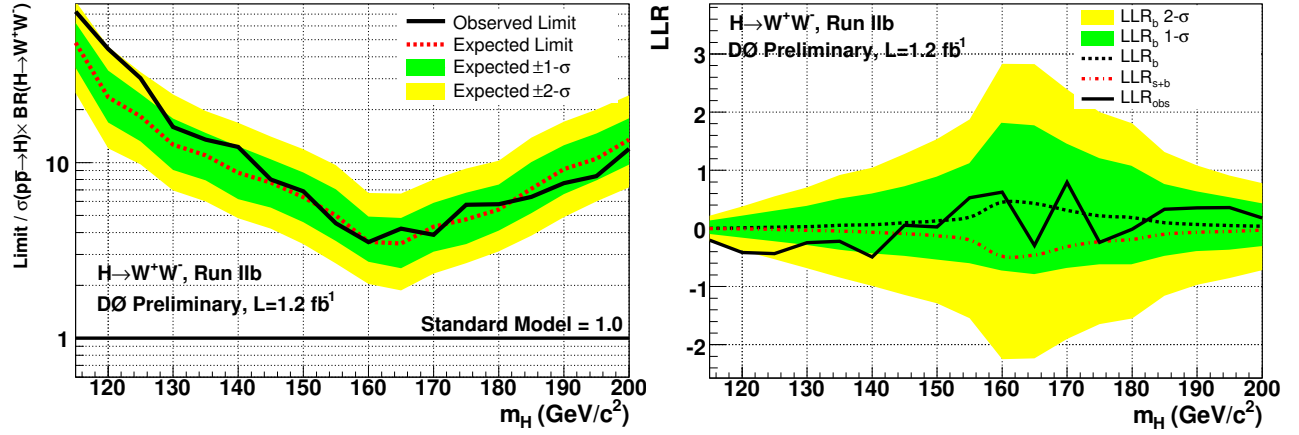[6] J. Elmsheuser, M. Hohlfeld, Phys. Rev. Lett. 96, 011801 (2006).

FIG. 9: Excluded cross section times branching ratio $\sigma \times BR(H \to WW^{(*)})$ at 95% CL in units of the SM cross section (left) and LLR (right) for all three channels combined, using 1.2 fb^{-1} of Run IIb data.
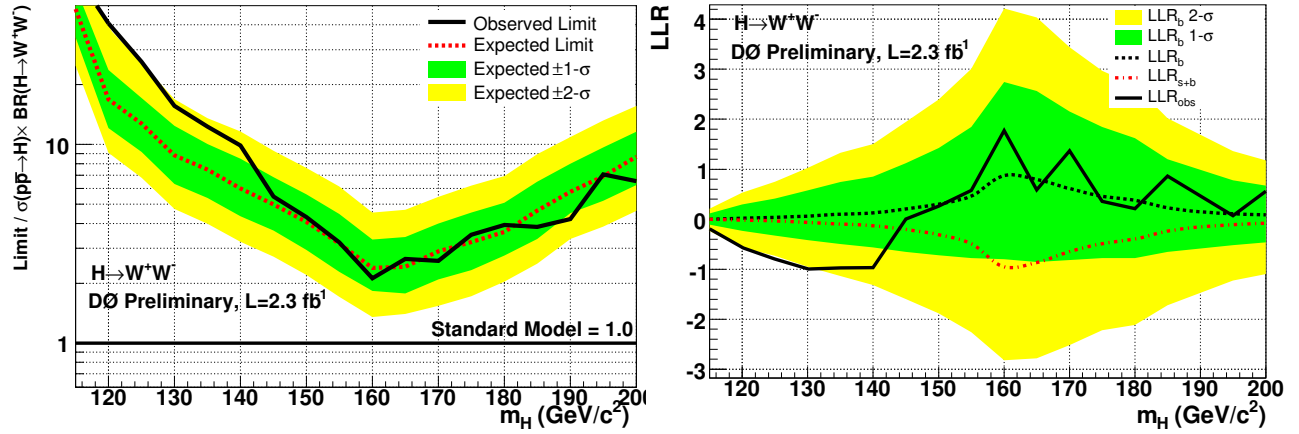

FIG. 10: Excluded cross section times branching ratio $\sigma \times BR(H \to WW^{(*)})$ at 95% CL in units of the SM cross section (left) and LLR (right) for all three channels combined, using the full 2.3 fb^{-1} of Run II data.

[7] DØ Collaboration, DØNote 5537, *Search for the Higgs Boson in $H \to WW^{(*)} \to \ell\ell'$ ($\ell, \ell' = e, \mu$) decays with up to 1.7 fb^{-1} at DØ in Run II*, (2007).
[8] DØ Collaboration, V. Abazov *et al.*, Nucl. Instrum. Methods Phys. Res. A. **565**, 463 (2006).
[9] DØ Collaboration, S. Abachi *et al.*, Nucl. Instrum. Methods Phys. Res. A **338**, 185 (1994).
[10] V. Abramov *et al.*, Nucl. Instrum. Methods Phys. Res. A. **419**, 660 (1998).
[11] T. Sjöstrand *et al.*, Comp. Phys. Comm. **135**, 238 (2001).
[12] M.L. Mangano, M. Moretti, F. Piccinini, R. Pittau, A. Polosa, JHEP 0307:001,2003, hep-ph/0206293.
[13] J. Pumplin et al., J. High Energy Phys. 07 (2002) 012.
[14] R. Brun and F. Carminati, CERN Program Library Long Writeup W5013, 1993 (unpublished).
[15] R. Hamberg, W.L. van Neerven, and T. Matsuura, Nucl. Phys. **B359**, 343 (1991) [Erratum-ibid. **B644**, 403 (2002)].
[16] T. Nunnemann, DØNote 4476.
[17] N. Kidonakis and R. Vogt, Phys. Rev. D **68**, 114014 (2003).
[18] J. M. Campbell and R. K. Ellis, Phys. Rev. D **60**, 113006 (1999).
[19] T. Gleisberg, F. Krauss, A. Schalicke, S. Schumann and J. C. Winter, Phys. Rev. D **72**, 034028 (2005).
[20] T. Junk, Nucl. Instrum. Methods Phys. Res. A. **434**, 435 (1999). A. Read, CERN 2000-005 (30 May 2000).
[21] W. Fisher, FERMILAB-TM-2386-E.